Water Supply

IWA PUBLISHING

Water Supply Vol 22 No 3, 2560 doi: 10.2166/ws.2021.450

Leak location procedure based on the complex-valued FastICA blind deconvolution algorithm for water-filled branch pipe

Mingyang Liu†, Jin Yang*, Endong Fan†, Jing Qiu and Wei Zheng

Key Laboratory of Optoelectronic Technology & System of China Education Ministry, Chongqing University, Chongqing 400044, China
*Corresponding author. E-mail: yangjin@cqu.edu.cn
†These authors contributed equally to this work.

JQ, 0000-0001-5163-2153

ABSTRACT

Water pipe networks have a large number of branch joints. Branch joint shunting generates vortices in the fluid, which excite the pipe wall to produce a type of branch noise. The branch noise is coupled with the leak source signal through the pipe. Here, a novel leak location protocol based on the complex-valued FastICA method (C-FastICA) is proposed to address the leak location problem under the branch noise interference. The C-FastICA, a complex-value domain blind deconvolution algorithm, effectively extended the cost function, constraint function, and iteration rules of the instantaneous linear FastICA into the complex-valued domain. The C-FastICA method was used to realize the separation of branch noise and leak source signal. The experimental results showed that the separation efficiency of the C-FastICA was higher than that of time-domain blind convolution separation (T-BCS). Furthermore, the relative location error of the C-FastICA method to the leak point was less than 14.238%, which was significantly lower than in traditional T-BCS and direct cross-correlation (DCC) technology.

Key words: branch noise, C-FastICA, DCC, leak location, T-BCS

HIGHLIGHTS

- The paper proposed a procedure based on the complex-valued FastICA method (C-FastICA) to address the leak location problem under the branch noise interference.
- The accuracy of the proposed C-FastICA leak location method is higher than the traditional cross-correlation location technology and time-domain deconvolution leak location technology.

1. INTRODUCTION

Leaks in water supply pipelines not only cause economic losses and environmental pollution, but also endanger the health and safety of urban residents. The main causes of pipe leaks are pipeline aging, chemical corrosion, external force damage, and management and maintenance negligence. According to the 'In-depth Investigation and Investment Prospect Analysis Report of China's Urban Water Supply Industry for 2020–2026' (Zhiyan Consulting 2019), the annual average rate of pipe leak in mainland China is 15.3% and some cities even exceed 25%, which is higher than the standard in many developed countries.

The acoustic emission (AE) detection method (Kim & Lee 2009; Brennan *et al.* 2016; Gao *et al.* 2017; Almeida *et al.* 2018; Kassab *et al.* 2019; Xiao *et al.* 2020) is widely used in detection of pipe leaks due to its low cost, non-intrusiveness, and high efficiency. The classic AE pipe detection is shown in Figure 1; the acoustic or vibration sensors are closely attached to both ends of the leak pipe to capture the leak signals. However, in real-world leak detection, various external and internal noises may interfere with the AE leak signal. External noises include those generated by automobiles, machines, and humans, whereas the internal noises are mainly caused by branch joints, elbow joints, valve joints, and other pipe joints. To effectively remove noise interference, Ahadi & Bakhtiar (2010) proposed a new method that captures the leak sound signal-signature in time domain based on the Short Time Fourier Transforms (STFT). The leak point was then located in the time-frequency domain using the tuned wavelet method. In a different study by Ting *et al.* (2021), a shift-invariant Dual Tree Complex Wavelet Transform (DTCWT) was used to remove noise interference in water pipe leak locations. Jafari *et al.* (2020) used an

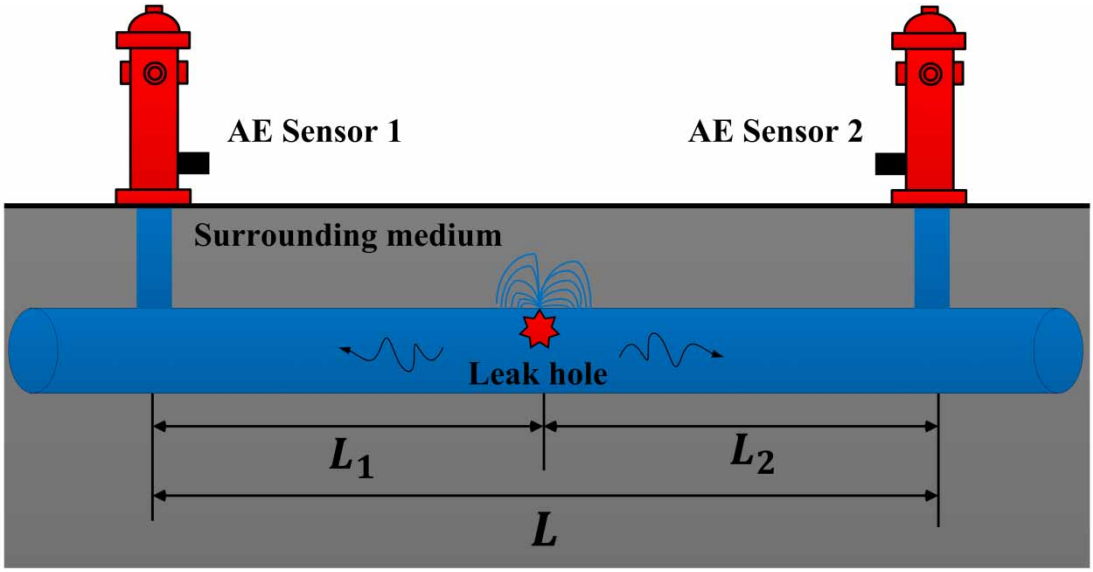

Figure 1 | Classic acoustic emission detection schematic.

extension version of Kalman filter observer to detect and locate the blockage in the pipeline. Saqib *et al.* (2017) used a wavelet-based adaptive thresholding scheme to restrain the noise inter-ference within the AE leak signals. Taghvaei *et al.* (2006) used a cepstrum analysis to detect and locate leaks in pipeline networks.

Butterfield *et al.* (2017) investigated the correlation between the leak flow rate and signal processing techniques such as the Vibro-Acoustic Emission (VAE) counts, signal Root Mean Square (RMS), peak in magnitude of the power spectral density, and octave banding. The results showed a strong correlation between the RMS and leak flow rate, prompting the development of a flow prediction model that was based on the RMS parameters. Subsequently, Mostafapour & Davoudi (2013) used the Donnell's non-linear theory, Galerkin method, and Runge–Kutta numerical method to develop an AE model induced by pipe leak vibration. Yu & Li (2017) proposed an experimental investigation into the detection of minor leaks. The time-domain waves, frequency, and energy features of the AE signals were first extracted and compared, before applying the SVM to recognize the minor leaks in the extracted features. In general, these de-noise methods are the procedure of removing or suppressing additive noise. However, these methods have two drawbacks. Firstly, environmental variables in actual leak detection conditions impact the mathematical models, interfering with the task and potentially leading to premature completion. Secondly, these methods generally capture leak signals from a straight leak pipe that is devoid of branch joints, and they consider mixed leak signals to be equivalent to the superposition of noise and leak sources.

In leak conditions, the mixed sound signal propagates along the pipe wall after the coupling and superimposing of pipe noise and the leak sound signal. Since the propagation mechanism is a convolutional process, the leak signal containing the pipe noise should be separated using a deconvolution method. All the noise generated by the pipe shape, including the noise caused by the branch flow, is a type of posterior noise with unknown time domain, frequency domain, and probability density characteristics. Therefore, the above-mentioned methods are mainly based on power spectrum characteristics, time-frequency characteristics, and other prior noise information that can be established or hypothesized to realize the AE signal processing analysis. Accordingly, the highlighted methods and techniques cannot be directly applied to eliminate branch noise because of the limited amount of prior knowledge of branch type leak detection. In addition, the branch noise and leak source signal have a convolution relationship with the propagation channel (pipe wall). Therefore, isolating the leak source signal from the branch-noise containing leak signal is a typical blind deconvolution separation (BSS) problem (Sun *et al.* 2015). Without knowing the probability density characteristic, time-domain and frequency-domain characteristics of the leak source signal and the branch noise signal, the blind separation algorithm can still complete the separation of the observation signal (leak mixing signal) obtained by the sound sensor.

In blind separation, FastICA is widely used due to its fast convergence and high separation precision. Therefore, to efficiently extract the leak source signal from the mixed leak signal containing branch noise, this paper proposes a leak detection procedure that is based on the complex-valued FastICA method (C-FastICA). As an improved algorithm of FastICA,

C-FastICA effectively extends the cost function, constraint function, and iteration rules of FastICA to the complex-valued domain. In section two of this paper, a computational fluid dynamics (CFD) example is used to describe the current problem in leak location of branch pipe. Section three briefly introduces the C-FastICA theory. Section four covers the leak location experiment, and conclusions are made in section five.

2. PROBLEM DESCRIPTION

The branch joint that connects a branch pipe to the main pipeline system changes the flow state of the fluid thus generating water eddies near the branch joint. The eddies excite the pipe wall, resulting in a kind of vortex-induced noise referred to in this paper as branch noise. This kind of branch noise has unsteady-state characteristics and can be regarded as an unsteady-state acoustic response caused by branch joint (Wang *et al.* 2005; Meniconi *et al.* 2021).

In this section, the computational fluid dynamics (CFD) software from ANSYS Fluent was used to simulate the eddy phenomenon in leak pipe with a branch joint (Figure 2). In preparatory work, the CAD model of leak pipe was built using SolidWorks 2014 software. The three-dimensional mesh was then generated using the ICEM software based on the CAD pipe model. The Fluent software provides a transient large eddy simulation (LES) solver. In calculation, a LES model was selected to simulate the steady flow field. The simulation was performed on a server called Dell Precision T7600 with an Intel Xeon (R) CPU E5-2678 W 0 at 3.10 GHz (16 CPUs) and 128 GB RAM. After the simulated calculation reached a steady state, we used CFD-Post software to post-process the calculation results.

Figure 3 shows the distribution of vortex core near the branch joint at four different moments: t = 500 steps, t = 1000 steps, t = 1500 steps, and t = 2000 steps. Figure 3 shows that as the time step increases, the maximum of fluid velocity displays a decreasing trend. According to the definition of vorticity in $\boldsymbol{\omega} = \nabla \times \boldsymbol{v}$, where $\boldsymbol{\omega}$ is vorticity of vortex core, ∇ is the Hamiltonian, $\boldsymbol{v}$ is the rotational velocity of the fluid, the vorticity is positively correlated with the fluid velocity, and the decrease in velocity leads to a decrease in vorticity. Due to the existence of this dynamically vortex core changing (as shown within the small black rectangle), the tube wall is excited to vibrate and to form vortex-induced noise, more details about vortex-induced noise are described in the literature (Chu 2006; Zhang *et al.* 2015; Zhang *et al.* 2016). This vortex-induced noise is mixed with the leak signal source and collected by a sensor installed on the pipeline, which becomes a major interference source for leak detection. Thus, we inferred that the leak detection will inevitably be interfered with due to the existence of one or more branch joints.

3. THE LEAK LOCATION METHOD BASED ON C-FASTICA ALGORITHM

3.1. Building convolution model for leak

In pipe leak accidents, the branch noise is coupled with the leak source signal through the pipe wall, and the leak mixed signal is then superimposed on the background noise to be acquired by a sound sensor. The background noise is mainly composed of environmental noise outside the pipeline, which is additive to the leak mixed signal (Ting *et al.* 2021; Deep *et al.* 2022). The mathematical analysis formula of the leak model is as follows:

$$\begin{cases} \boldsymbol{x}_1(n) = \boldsymbol{a}(n) * s(n) + \boldsymbol{n}_1(n) \\ \boldsymbol{x}_2(n) = \boldsymbol{b}(n) * s(n) + \boldsymbol{n}_2(n) \end{cases} \tag{1}$$

where $\boldsymbol{x}_1(n)$ and $\boldsymbol{x}_2(n)$ are $d \times N$ observation matrices acquired from two sensors; $\boldsymbol{a}(n)$ and $\boldsymbol{b}(n)$ are two different $d \times d$ transfer matrices; $\boldsymbol{s}(n)$ is the unknown $d \times$ N mixing source matrix, $\mathbf{s}(n) = \boldsymbol{s}_{leak}(n) + \boldsymbol{s}_{branch}(n)$; $\boldsymbol{s}_{leak}(n)$ is leak source; $\boldsymbol{s}_{branch}(n)$ is branch noise; and $\boldsymbol{n}_1(n)$ and $\boldsymbol{n}_2(n)$ are the random interference factors. To further simplify Equation (1), we transformed

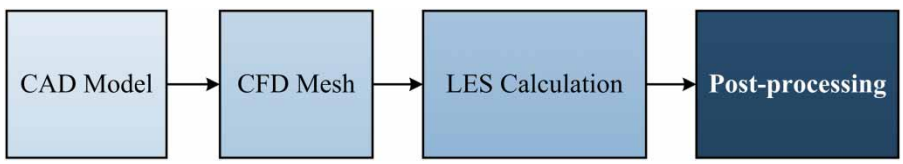

Figure 2 | CFD simulation flow chart for leak pipe with a branch joint.

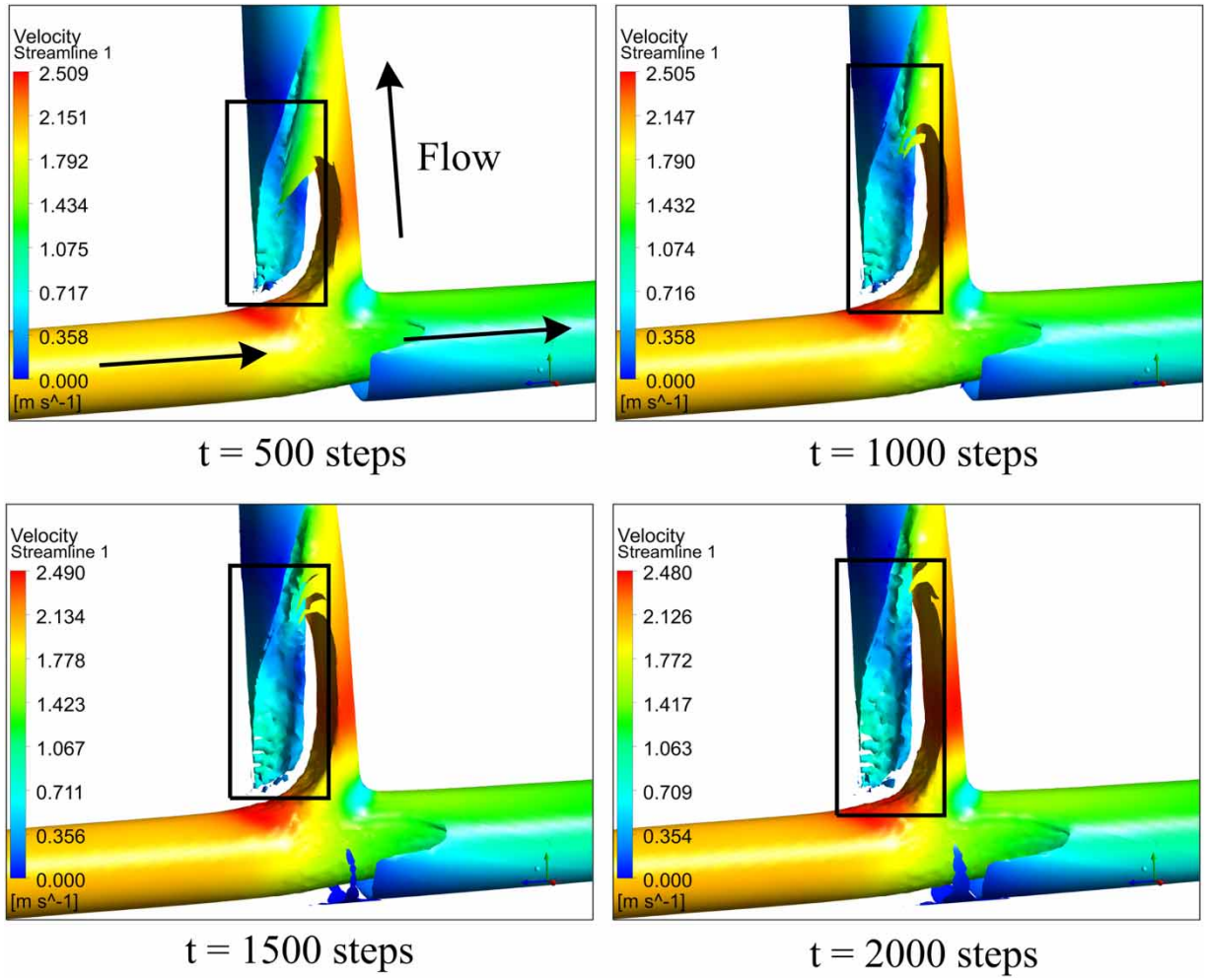

Figure 3 | Illustration of vortex core distribution near branch joint.

its time domain to frequency domain, resulting in the product form of Equation (1):

$$\begin{cases} \boldsymbol{X}_1(z) = \boldsymbol{A}(z)\boldsymbol{S}(z) + \boldsymbol{N}_1(z) \\ \boldsymbol{X}_2(z) = \boldsymbol{B}(z)\boldsymbol{S}(z) + \boldsymbol{N}_2(z) \end{cases} \tag{2}$$

Usually, the z is omitted:

$$\begin{cases} \boldsymbol{X}_1 = \boldsymbol{A}\boldsymbol{S} + \boldsymbol{N}_1 \\ \boldsymbol{X}_2 = \boldsymbol{B}\boldsymbol{S} + \boldsymbol{N}_2 \end{cases} \tag{3}$$

In the frequency domain, the convolutional mixing model was transformed into a linear instantaneous mixing model, and the C-FastICA was used to separate the mixed signal. Following the completion of the calculations, the frequency domain results were converted into time-domain sources, as shown in Figure 4.

3.2. Background of the C-FastICA method

C-FastICA is a complex-valued extension form of FastICA, where the cost function, constraint function, and iterative learning rules of FastICA are effectively extended to the complex-valued domain. In the complex-valued domain, the source signal, mixed signal, and unmixing matrix are all in a complex form, and they are represented as follows:

$$\begin{cases} s = \boldsymbol{s}_r + j\boldsymbol{s}_i \\ x = \boldsymbol{x}_r + j\boldsymbol{x}_i \\ W = \boldsymbol{W}_r + j\boldsymbol{W}_i \end{cases} \tag{4}$$

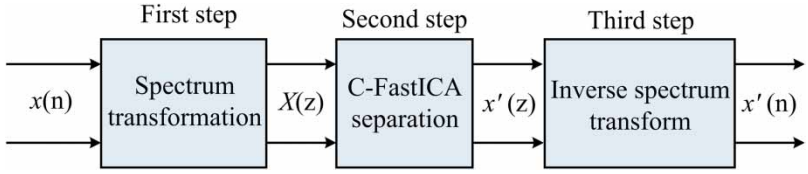

Figure 4 | Blind separation sketch of convolutive mixtures in frequency-domain.

where $\boldsymbol{s}$ is the source signal, $\boldsymbol{s}_{\mathbf{r}}$ is the real part of $\boldsymbol{s}$, and $\boldsymbol{s}_{\mathbf{i}}$ is the imaginary part of $\boldsymbol{s}$; $\boldsymbol{x}$ is the mixed signal, $\boldsymbol{x}_{\mathbf{r}}$ is the real part of $\boldsymbol{x}$, and $\boldsymbol{x}_{\mathbf{i}}$ is the imaginary part of $\boldsymbol{x}$; $\boldsymbol{W}$ is the unmixing matrix, and $\boldsymbol{W}_{\mathbf{r}}$ is the real part of $\boldsymbol{W}$, $\boldsymbol{W}_{\mathbf{i}}$ is the imaginary part of $\boldsymbol{W}$. According to the Kuhn-Tucker conditions (Lv *et al.* 2007), under the constraint condition $E((\boldsymbol{W}^H\boldsymbol{x})^2) = \|\boldsymbol{W}\|^2 = 1$, the maximum cost function $E(G|\boldsymbol{W}^H\boldsymbol{x}|^2)$ was obtained by the first order derivative of the following formula:

$$\nabla E(G|\boldsymbol{W}^H\boldsymbol{x}|^2) - \beta\nabla E(|\boldsymbol{W}^H\boldsymbol{x}|^2) = 0 \tag{5}$$

where $G(\cdot)$ is the nonlinear function, it is defined as $G(x) = \lg(0.1 + x)$. Next, we differentiated the real and imaginary parts of $\boldsymbol{W}$ in Equation (5). The first term on the left side of Equation (5) can be written as:

$$\nabla E(G|\boldsymbol{W}^H\boldsymbol{x}|^2) = 2\begin{pmatrix} E(\mathrm{Re}(x_1(\boldsymbol{W}^H)^*)g(|\boldsymbol{W}^H\boldsymbol{x}|^2)) \\ E(\mathrm{Im}(x_1(\boldsymbol{W}^H)^*)g(|\boldsymbol{W}^H\boldsymbol{x}|^2)) \\ \cdots \\ E(\mathrm{Re}(x_n(\boldsymbol{W}^H)^*)g(|\boldsymbol{W}^H\boldsymbol{x}|^2)) \\ E(\mathrm{Im}(x_n(\boldsymbol{W}^H)^*)g(|\boldsymbol{W}^H\boldsymbol{x}|^2)) \end{pmatrix} \tag{6}$$

The * represents the complex conjugate. Equation (6) can be arranged as a vector form:

$$\nabla E(G|\boldsymbol{W}^H\boldsymbol{x}|^2) = 2E(\boldsymbol{x}(\boldsymbol{W}^H\boldsymbol{x})^* g(|\boldsymbol{W}^H\boldsymbol{x}|^2)) \tag{7}$$

The second term on the left side of Equation (5) can be written as:

$$\beta\nabla E(|\boldsymbol{W}^H\boldsymbol{x}|^2) = 2\beta(\mathrm{Re}(\boldsymbol{W}_1), \mathrm{Im}(\boldsymbol{W}_1), \ldots, \mathrm{Re}(\boldsymbol{W}_n), \mathrm{Im}(\boldsymbol{W}_n))^T \tag{8}$$

We used the Newton iteration method (Chen 2017) to solve the optimization results of Equation (5). In the first step, we presented the Jacobian matrix approximate form of the matrix $\nabla E(G|\boldsymbol{W}^H\boldsymbol{x}|^2)$ in Equation (5):

$$\nabla^2 E(G|\boldsymbol{W}^H\boldsymbol{x}|^2) \approx 2E(g(|\boldsymbol{W}^H\boldsymbol{x}|^2) + |\boldsymbol{W}^H\boldsymbol{x}|^2 g'(|\boldsymbol{W}^H\boldsymbol{x}|^2))\boldsymbol{I} \tag{9}$$

Then, like in the first step the Jacobian matrix approximate form of the matrix $\beta\nabla E(|\boldsymbol{W}^H\boldsymbol{x}|^2)$ was:

$$\beta\nabla^2 E(|\boldsymbol{W}^H\boldsymbol{x}|^2) = 2\beta\boldsymbol{I} \tag{10}$$

Combining Equations (9) and (10) resulted in the Jacobian matrix of the cost function Equation (5) as follows:

$$J = 2(E(g(|\boldsymbol{W}^H\boldsymbol{x}|^2) + |\boldsymbol{W}^H\boldsymbol{x}|^2 g'(|\boldsymbol{W}^H\boldsymbol{x}|^2)) - \beta)\boldsymbol{I} \tag{11}$$

The Newton iteration method was used to iterate on Equation (11):

$$\boldsymbol{W}^+ = \boldsymbol{W} - \frac{E(\boldsymbol{x}(\boldsymbol{W}^H\boldsymbol{x})^* g(|\boldsymbol{W}^H\boldsymbol{x}|^2)) - \beta\boldsymbol{W}}{E(g(|\boldsymbol{W}^H\boldsymbol{x}|^2) + |\boldsymbol{W}^H\boldsymbol{x}|^2 g'(|\boldsymbol{W}^H\boldsymbol{x}|^2)) - \beta} \tag{12}$$

We multiplied both sides of Equation (12) by $[-E(g(|\boldsymbol{W}^H\boldsymbol{x}|^2)+|\boldsymbol{W}^H\boldsymbol{x}|^2 g'(|\boldsymbol{W}^H\boldsymbol{x}|^2))+\beta]$, thus, the iterative learning rule for solving the mixing matrix $\boldsymbol{W}$ was obtained as follows:

$$\boldsymbol{W}^+ = E(\boldsymbol{x}(\boldsymbol{W}^H\boldsymbol{x})^* g(|\boldsymbol{W}^H\boldsymbol{x}|^2)) - E(g(|\boldsymbol{W}^H\boldsymbol{x}|^2)+|\boldsymbol{W}^H\boldsymbol{x}|^2 g'(|\boldsymbol{W}^H\boldsymbol{x}|^2))\boldsymbol{W} \tag{13}$$

Moreover, in order to avoid the uncertainty of the output vector amplitude, the $\boldsymbol{W}^+$ obtained at each step was normalized:

$$\boldsymbol{W}^+_{new} = \frac{\boldsymbol{W}^+}{\|\boldsymbol{W}^+\|} \tag{14}$$

Finally, by combining Equations (10) and (11), the time domain algorithm of FastICA was successfully extended to the complex-valued domain, that is, the instantaneous linear blind separation iterative learning rule of C-FastICA was obtained. Then we calculated the frequency-domain decomposition result of the mixed signal $\boldsymbol{x}$:

$$(\boldsymbol{y})_f = (\boldsymbol{W}^+_{new})_f \boldsymbol{x}_f \tag{15}$$

where$(\boldsymbol{y})_f$ is the frequency-domain output estimation, the $\boldsymbol{x}_f$ is frequency-domain source signal, $\boldsymbol{W}_f$ is the frequency-domain unmixing matrix. After the calculation of Equation (12), we transformed the complex-valued output $(\boldsymbol{y})_f$ into the time domain:

$$(\boldsymbol{y})_t \leftarrow IFFT(\boldsymbol{y})_f \tag{16}$$

where $(\boldsymbol{y})_t$ is the time-domain output estimation, the proposed C-FastICA is summarized in Algorithm 1.

Algorithm 1: Complex- valued FastICA (C-FastICA)

(1). The time-domain observation signal $x(n)$ is transformed to complex-valued form through FFT: $\boldsymbol{x} = x_r + \boldsymbol{j}x_i$;

(2). Initialize $\boldsymbol{W} = \text{randn}(2, 2) + \boldsymbol{j} \cdot \text{randn}(2, 2)$;

(3). According to the definition $G(\boldsymbol{x}) = \lg(0.1 + \boldsymbol{x})$, calculate the $g(\boldsymbol{x}) = 1/(0.1 + \boldsymbol{x})$ and $g(\boldsymbol{x}) = -1/(0.1 + \boldsymbol{x})^2$;

(4). Initialize $\boldsymbol{W}^+$ using Equation (12);

(5). For iter ≥ 0:

Calculate

$\boldsymbol{W}^+ = E(\boldsymbol{x}(\boldsymbol{W}^H\boldsymbol{x})^* g(|\boldsymbol{W}^H\boldsymbol{x}|^2)) - E(g(|\boldsymbol{W}^H\boldsymbol{x}|^2)+|\boldsymbol{W}^H\boldsymbol{x}|^2 g'(|\boldsymbol{W}^H\boldsymbol{x}|^2))\boldsymbol{W}$, $\boldsymbol{W}^+_{new} = \frac{\boldsymbol{W}^+}{\|\boldsymbol{W}^+\|}$

(6). End for convergence: $(\boldsymbol{y})_f = \boldsymbol{W}_f^+ \boldsymbol{x}_f$.

(7). Cross-correlation estimation: $\tau = \int_{-\infty}^{\infty} \boldsymbol{y}(t)\boldsymbol{y}^*(t+\tau_0)dt$

(8). Leak location: $L_1 = (L - c\tau)/2$

4. LEAK LOCATION EXPERIMENT

The main leak location steps are shown in Figure 5, and are listed below as used in the experiment:

Step 1: two mixing leak signal $\boldsymbol{x}_1$(n) and $\boldsymbol{x}_2$(n) were acquired by acceleration sensors.

Step 2: the obtained $\boldsymbol{x}_1$(n) and $\boldsymbol{x}_2$(n) were transformed into frequency domain, then, two frequency-domain signals $\boldsymbol{x}_1(f)$ and $\boldsymbol{x}_2(f)$ were obtained.

Step 3: the $\boldsymbol{x}_1(f)$ and $\boldsymbol{x}_2(f)$ were treated as input for C-FastICA separation, and the unmixing matrixes $\boldsymbol{W}_1(f)$ and $\boldsymbol{W}_2(f)$ were calculated.

Step 4: we further computed the output $y_1(f)$ and $y_2(f)$ based on the unmixing matrixes $\boldsymbol{W}_1(f)$ and $\boldsymbol{W}_2(f)$.

Step 5: the output $y_1(f)$ and $y_2(f)$ were transformed into time domain, then, the time-domain output $y_1(t)$ and $y_2(t)$ were obtained.

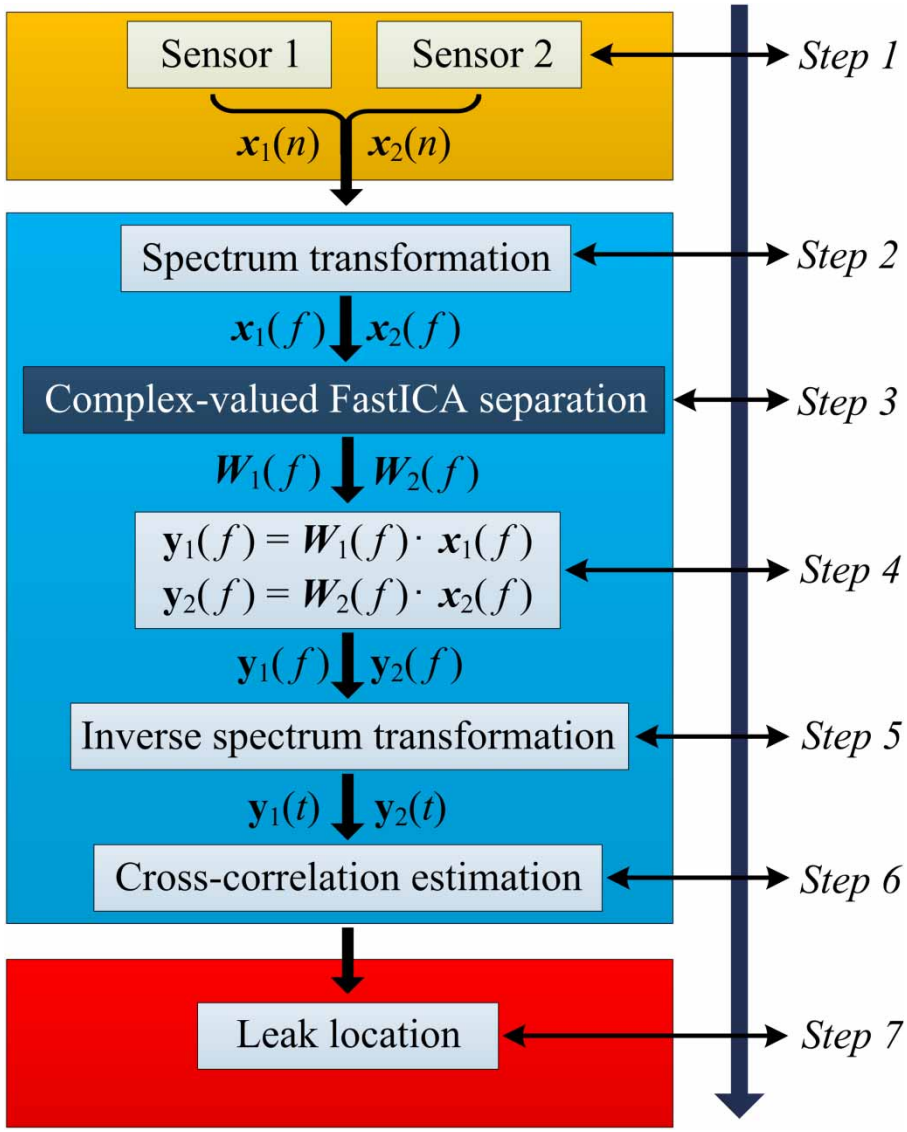

Figure 5 | Flowchart of the leak location in the branch pipeline system.

Step 6: the cross-correlation method was used to obtain the time delay estimation (TDE) based on the obtained $y_1(t)$ and $y_2(t)$ in step 5.

Step 7: we combined the known distance $L = 70$ m, TDE, and the empirical leak sound velocity $c = 1495$ m/s to complete the leak location task.

4.1. Conditions of the experiment

In this section, we used the acceleration sensors to collect two mixing leak signals containing branch noise, which were then separated using the C-FastICA algorithm. We selected a cast iron water supply pipe with a diameter of 100 mm and a test length of 70 m for the experiment. The branch node has water consumption in the corresponding branch pipeline. The pipe inner pressure was 0.6 MPa, and the inlet flow rate was approximately 2 m/s. The simulated leak point, which was 42 m away from sensor 1, was replaced by a small valve (leakage aperture = 15 mm) and the data sampling rate was set at 10 KHz. More details on the used parameters are shown in Table 1. A schematic diagram of the leak location experiment (Figure 6), and real diagrams of the two sensors and branch joints (Figure 7) are as shown below. Two sensors were placed at the different ends of the main pipe, and the collected leak signals were wirelessly transmitted to the host computer (Figure 6).

Table 1 | Detailed parameters of the experiment

Parameters	Values
Pipe diameter	100 mm
Leak valve diameter	15 mm
Test pipe length: $L_1 + L_2 + L_3$	70 m
L_1: Sensor 1 distance from the leak point	$L_1 = 42$ m
L_2: Branch joint distance from the leak point	$L_2 = 8$ m
L_3: Sensor 2 distance from the branch joint	$L_3 = 20$ m
Pipe inner pressure	0.6 MPa
Flow velocity	2 m/s
Sampling rate	10 KHz

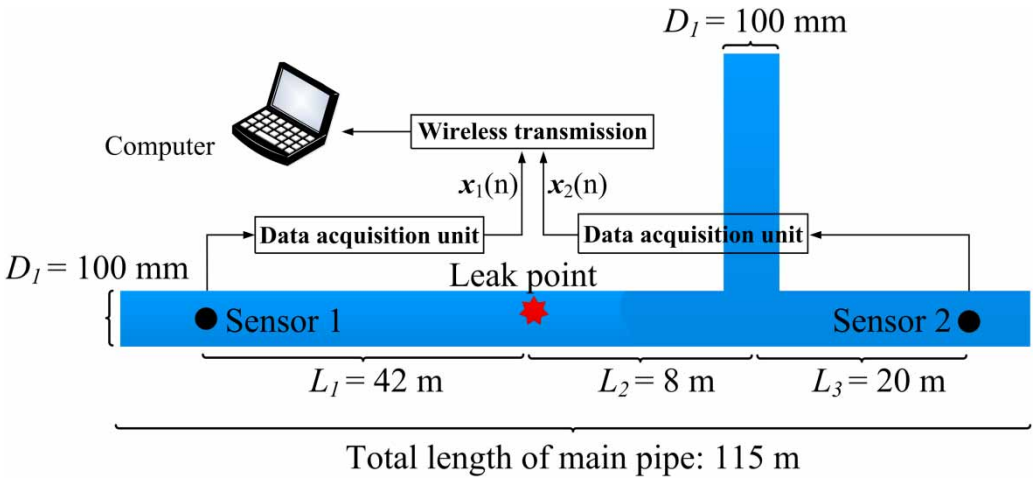

Figure 6 | Schematic of leak location experiment.

Figure 7 | Pictures of branch joint, Sensor 1 and Sensor 2.

4.2. Leak location processing

We chose the leak signal collected by Sensor 1 as an example, and used the C-FastICA algorithm to process it. The time-domain (Figure 8(a)) and frequency-domain (Figure 8(b)) forms of the leak signal containing branch noise are shown below.

To prove that the C-FastICA algorithm outperforms the traditional algorithm, we separated the mixing leak signal using the well-known time-domain blind convolution separation (T-BCS) algorithm. The signal had to be preprocessed before

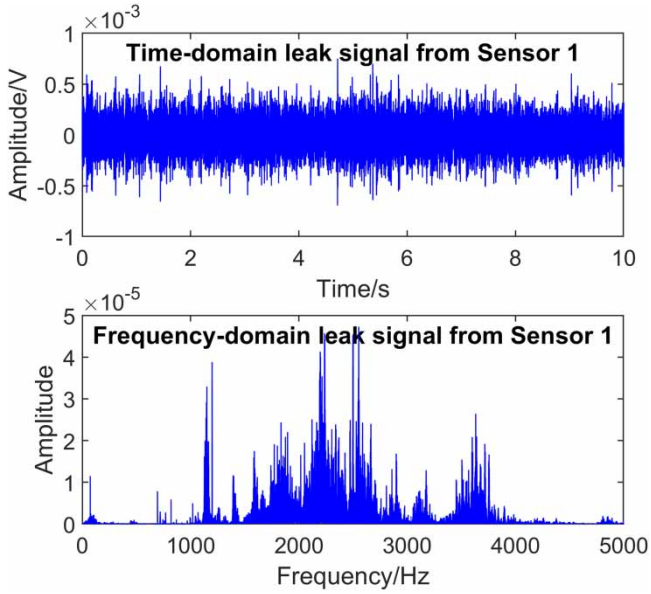

Figure 8 | (a) Time-domain leak signal from Sensor 1, (b) Leak signal power spectrum from Sensor 1.

separating the mixing leak signal to suppress the influence of the additive noise n_1 and n_2 in Equation (1). After removing the additive noise in the mixing leak signal, the leak acoustic source and branch noise are the main components in the mixing leak signal. Then, the C-FastICA was used to perform blind separation for the mixing leak signal in the frequency domain. For more information on suppressing the additive noise, see Bell & Sejnowski (1995). The C-FastICA algorithm revealed that the spectral components of y_1 and y_2 were mainly occupied in the range of 1700–2600 and 1100–4000 Hz, respectively (Figure 9(a)). The T-BCS algorithm results indicated that the spectral characteristics of y_1 and y_2 were between 1600–2200 and 1000–4000 Hz, respectively (Figure 9(b)). This denotes that y_2 has a wider frequency bandwidth than y_1. Therefore, we can infer from the previous leak theory(Diao *et al.* 2020; Scussel *et al.* 2021) that the randomness of the leak signal is often greater than that of other stable noise signals, except white noise, implying that the bandwidth of the leak source signal is wider than other noise signals. Consequently, we concluded that y_2 was the leak source signal obtained by the

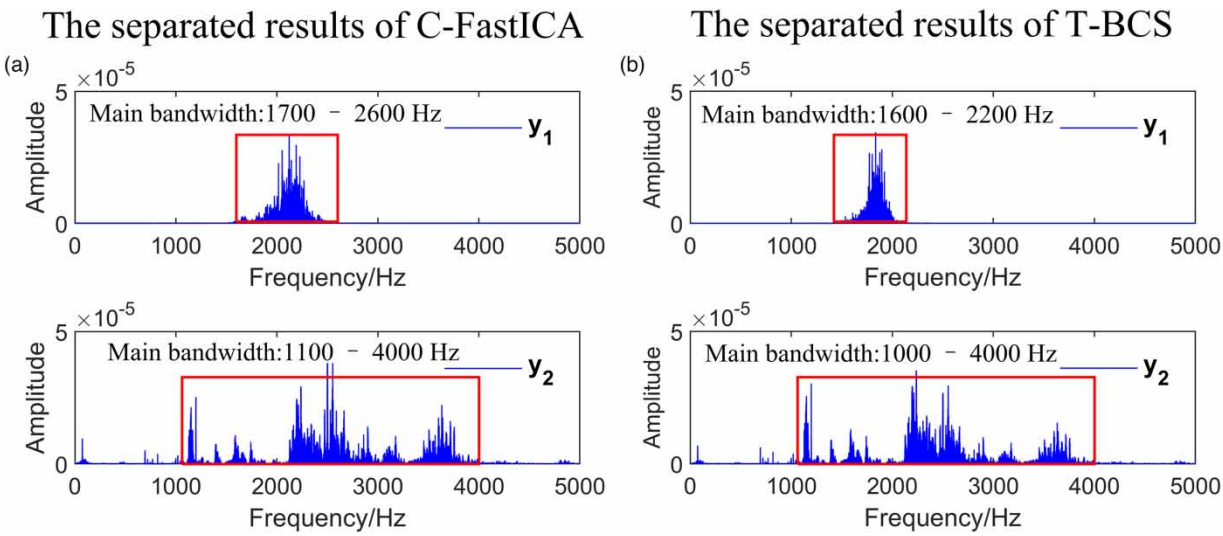

Figure 9 | Separated results of C-FastICA and T-BCS: (a) separated components y_1 and y_2 based on C-FastICA; (b) separated components y_1 and y_2 based on T-BCS.

separation algorithm, and y_1 was the branch noise. When the number of branch pipe nodes is more than one, there will be multiple narrow frequency components in the separation result, and these narrow frequency components are considered branch noise.

To evaluate the convergence speed of the algorithms, the inter-symbol interference (ISI) concept was introduced and defined as follows (Jenq 1979):

$$\mathrm{ISI}_i = \frac{\sum_i \sum_k |\boldsymbol{c}_{ij}|^2 - \max_{j,k}|\boldsymbol{c}_{i,j}(k)|^2}{\max_{j,k}|\boldsymbol{c}_{ij}(k)|^2} \tag{17}$$

where $\boldsymbol{c}_{ij}$ is the (i, j)th element in the global system matrix $\boldsymbol{C}$. The algorithm is more convergent when the ISI output curve of each channel is closer to zero. The ISI output curves indicated that each of the two channels converged at about 300 steps in C-FastICA (Figure 10(a)) and at about 400 steps in T-BCS (Figure 10(b)). Thus, convergence is faster in the C-FastICA algorithm than in T-BCS arigorithm.

The crosstalk error PI was introduced to compare the separated degree of the C-FastICA and the T-BCS. The closer the PI value is to zero, the higher the separation degree of the mixed signal. The PI was defined as follows (Leung & Siu 2007):

$$PI = \frac{1}{M(M-1)} \sum_{i=1}^{M} \left[\left(\sum_{k=1}^{M} \frac{|c_{ik}|}{\max_j |c_{ij}|} - 1 \right) + \left(\sum_{k=1}^{M} \frac{|c_{ki}|}{\max_j |c_{ji}|} - 1 \right) \right] \tag{18}$$

where M is the number of source components, c_{ik} is the element of $\boldsymbol{C} = \boldsymbol{W}\cdot\boldsymbol{A}$, $\boldsymbol{A}$ is the mixing matrix, and $\boldsymbol{W}$ is the separation matrix obtained by separation algorithms. The C-FastICA algorithm and the T-BCS algorithm were used to separate the leak signal containing the branch noise for another 50 times. It should be emphasized that the leak mixing signal and other specific experimental parameters used in these 50 times experiments remain the same. The PI results are shown in Figure 11.

The PI coefficients of C-FastICA algorithm were smaller, with a median value of about 0.192, than those of the T-BCS algorithm which had a median value of about 0.237 (Figure 11). Therefore, C-FastICA had a higher separation degree for the mixing leak signals, and the obtained leak source contained more leak characteristics. Following the separation calculation for the mixing leak signal collected by Sensor 1, we processed the mixing leak signal collected by Sensor 2 in the same way. The cross-correlation method was then used to obtain the TDE τ based on the two leak source signals:

$$\tau = \int_{-\infty}^{\infty} \boldsymbol{y}_2(t)\boldsymbol{y}_2^*(t+\tau_0)dt \tag{19}$$

where $y_2(t)$ and $y_2^*(t)$ are two leak sources obtained by blind separation, $y_2(t)$ is from Sensor 1, $y_2^*(t)$ is from Sensor 2, τ_0 is the delay parameter. The leak hole location was computed using the distance $L_1 = 42$ m, TDE τ, and the known leak sound

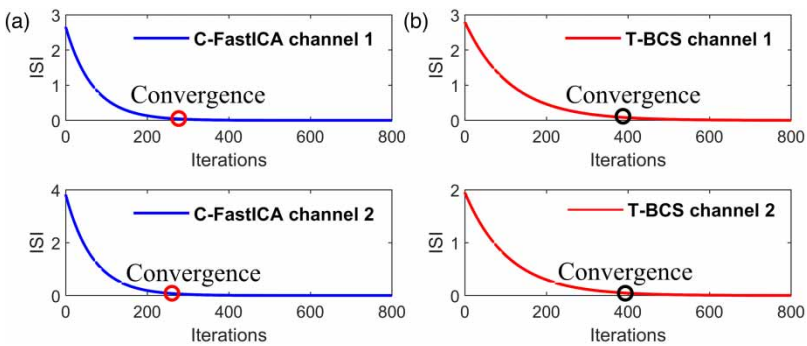

Figure 10 | ISI changes between C-FastICA channels and T-BCS channels.

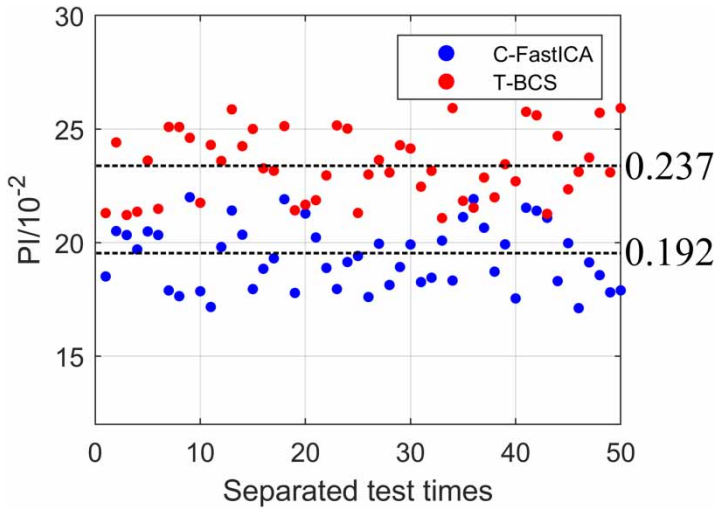

Figure 11 | PI values of C-FastICA and T-BCS were blind separated for 50 times.

velocity $c = 1495$ m/s as follows:

$$L_1 = (L - c\tau)/2 \tag{20}$$

where L is equivalent to $L_1 + L_2 + L_3 = 70m$. The peak value obtained using the C-FastICA algorithm (Figure 12(a)) was the closest to the true leak location compared to peak values shown by the T-BCS algorithm (Figure 12(b)) and the direct cross-correlation method (DCC; Figure 12(c)).

Since the branch noise was not removed before the analysis using the DCC method, it had a significant impact on the cross-correlation estimation thus yielding a leak location value with the largest error (Figure 12(c)) compared to the other two methods. To further verify that the separation performance of C-FastICA for mixed leak signals was better than T-BCS, this experiment was replicated eight times. The leak location results for each method are shown in Table 2. In the eight times leak location experiments in Table 2, eight acquisitions of leak mixing signal were carried out, the leak mixing signal used in each experiment is different.

The relative location error (δ) of C-FastICA did not exceed 14.238%, while in the T-BCS algorithm it reached 21.857%, indicating that C-FastICA algorithm had a higher position accuracy than T-BCS algorithm. However, noise had a significant impact on the DCC method whose relative error value was greater than 58%, and the leak location could not even be completed in numbers 2, 3, 6, 7, and 9.

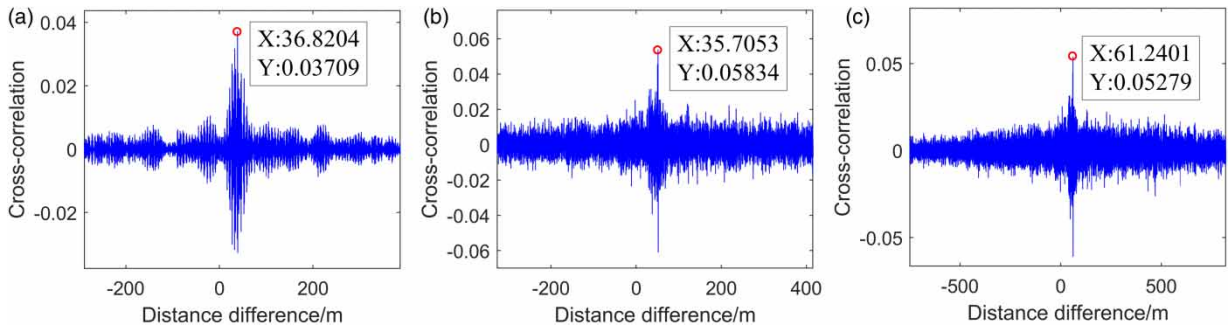

Figure 12 | (a) Leak location using the C-FastICA method, L_1 is equivalent to 36.82 m; (b) Leak location using the T-BCS method, L_1 is equivalent to 35.71 m; (c) Leak location using the DCC method, L_1 is equivalent to 61.24 m.

Table 2 | Leak location results based on C-FastICA, T-BCS and DCC

	C-FastICA		T-BCS		DCC	
Number	Distance (m)	δ (%)	Distance (m)	δ (%)	Distance (m)	δ (%)
1	36.82	12.333	35.71	14.976	61.24	45.810
2	36.95	12.024	34.07	18.881	NaN	NaN
3	37.05	11.786	34.59	17.643	NaN	NaN
4	37.54	10.619	**32.82**	**21.857**	58.96	40.381
5	37.12	11.619	33.29	20.738	**66.53**	**58.405**
6	36.76	12.476	35.17	16.262	NaN	NaN
7	**36.02**	**14.238**	34.69	17.405	NaN	NaN
8	37.33	11.119	34.18	18.619	56.82	35.286
9	37.98	9.571	35.02	16.619	NaN	NaN

5. CONCLUSION

This paper proposed the use of the C-FastICA method to separate the mixing leak signal and to solve the branch noise interference problem in the leak location of branch water pipes. Following the separation calculation, the leak sources were identified, and the leak location was completed by combining the prior leak sound velocity and the known pipe length. The feasibility of the proposed leak location method was proved through experiments, and the following conclusions were reached:

(1) When there was a branch joint in a water pipeline, the leak signal was mixed with the branch noise, and the T-BCS and DCC methods for locating the leak point had a significant error or were unable to complete the location. It shows that the influence of the branch noise cannot be ignored on the branch pipe leak location.
(2) The experiments proved that the C-FastICA algorithm has a faster convergence speed and a higher separation level for the mixed leak signals than the T-BCS algorithm.

ACKNOWLEDGEMENTS

This project was supported by the National Natural Science Foundation of China (No. 51675069), the National Natural Science Foundation of China (No. 51775070), and the Fundamental Research Funds for the Central Universities (Nos. 2018CDQYGD0020, cqu2018CDHB1A05).

DATA AVAILABILITY STATEMENT

Data cannot be made publicly available; readers should contact the corresponding author for details.

REFERENCES

Ahadi, M. & Bakhtiar, M. S. 2010 Leak detection in water-filled plastic pipes through the application of tuned wavelet transforms to Acoustic Emission signals. *Applied Acoustics* **71**, 634639. https://doi.org/10.1016/j.apacoust.2010.02.006.

Almeida, F. C. L., Brennan, M. J., Joseph, P. F., Gao, Y. & Paschoalini, A. T. 2018 The effects of resonances on time delay estimation for water leak detection in plastic pipes. *Journal of Sound and Vibration* **420**, 315–329. https://doi.org/10.1016/j.jsv.2017.06.025.

Bell, A. J. & Sejnowski, T. J. 1995 An information-maximization approach to blind separation and blind deconvolution. *Neural Computation* **7** (6), 1129–1159.

Brennan, M. J., Kroll De Lima, F., De Almeida, F. C. L., Joseph, P. F. & Paschoalini, A. T. 2016 A virtual pipe rig for testing acoustic leak detection correlators: proof of concept. *Applied Acoustics* **102**, 137–145. https://doi.org/10.1016/j.apacoust.2015.09.015.

Butterfield, J. D., Krynkin, A., Collins, R. P. & Beck, S. B. M. 2017 Experimental investigation into vibro-acoustic emission signal processing techniques to quantify leak flow rate in plastic water distribution pipes. *Applied Acoustics* **119**, 146–155. http://dx.doi.org/10.1016/j.apacoust.2017.01.002.

Chen, Y. Z. 2017 Evaluation of the degenerate scale in Laplace equation by using Newton iteration method. *Engineering Analysis with Boundary Elements* **80** (December 2016), 105–107. http://dx.doi.org/10.1016/j.enganabound.2017.02.013.

Chu, A. K. H. 2006 Passive transport of atomic gases within a vortex tube induced by a noise wave. *Physics Letters, Section A: General, Atomic and Solid State Physics* **349** (1–4), 135–145.

Deep, K., Fong, S. & Narasimhan, S. 2022 Active acoustic leak detection and localization in a plastic pipe using time delay estimation. *Applied Acoustics* **187**, 108482. https://doi.org/10.1016/j.apacoust.2021.108482.

Diao, X., Jiang, J., Shen, G., Chi, Z., Wang, Z., Ni, L., Mebarki, A., Bian, H. & Hao, Y. 2020 An improved variational mode decomposition method based on particle swarm optimization for leak detection of liquid pipelines. *Mechanical Systems and Signal Processing* **143**, 106787. https://doi.org/10.1016/j.ymssp.2020.106787.

Gao, Y., Brennan, M. J., Liu, Y., Almeida, F. C. L. & Joseph, P. F. 2017 Improving the shape of the cross-correlation function for leak detection in a plastic water distribution pipe using acoustic signals. *Applied Acoustics* **127**, 24–33. http://dx.doi.org/10.1016/j.apacoust.2017.05.033.

Jafari, R., Razvarz, S. & Gegov, A. 2020 Blockage detection in pipeline based on the extended kalman filter observer. *Electronics* **9** (91), 161–174. http://dx.doi.org/10.3390/electronics9010091.

Jenq, Y. C. 1979 Probability of error in digital fiber optic systems with inter-symbol interference and signal dependent additive noise. *Journal of the Franklin Institute* **307** (5), 291–303. https://www.sciencedirect.com/science/article/pii/0016003279900334.

Kassab, S., Michel, F. & Maxit, L. 2019 Water experiment for assessing vibroacoustic beamforming gain for acoustic leak detection in a sodium-heated steam generator. *Mechanical Systems and Signal Processing* **134**, 106332. https://doi.org/10.1016/j.ymssp.2019.106332.

Kim, M. S. & Lee, S. K. 2009 Detection of leak acoustic signal in buried gas pipe based on the time-frequency analysis. *Journal of Loss Prevention in the Process Industries* **22** (6), 990–994. http://dx.doi.org/10.1016/j.jlp.2008.08.009.

Leung, C. T. & Siu, W. C. 2007 A general contrast function based blind source separation method for convolutively mixed independent sources. *Signal Processing* **87** (1), 107–123.

Lv, Y., Hu, T., Wang, G. & Wan, Z. 2007 A penalty function method based on Kuhn-Tucker condition for solving linear bilevel programming. *Applied Mathematics and Computation* **188** (1), 808–813.

Meniconi, S., Cifrodelli, M., Capponi, C., Duan, H.-F. & Brunone, B. 2021 Transient response analysis of branched pipe systems toward a reliable skeletonization. *Journal of Water Resources Planning and Management* **147** (2), 04020109.

Mostafapour, A. & Davoudi, S. 2013 Analysis of leakage in high pressure pipe using acoustic emission method. *Applied Acoustics* **74** (3), 335–342. http://dx.doi.org/10.1016/j.apacoust.2012.07.012.

Saqib, N. U., Mysorewala, M. F. & Cheded, L. 2017 A novel multi-scale adaptive sampling-based approach for energy saving in leak detection for WSN-based water pipelines. *Measurement Science and Technology* **28** (12), 125102.

Scussel, O., Brennan, M. J., Almeida, F. C. L., Muggleton, J. M., Rustighi, E. & Joseph, P. F. 2021 Estimating the spectrum of leak noise in buried plastic water distribution pipes using acoustic or vibration measurements remote from the leak. *Mechanical Systems and Signal Processing* **147**, 107059. https://doi.org/10.1016/j.ymssp.2020.107059.

Sun, J., Xiao, Q., Wen, J. & Yang, Y. 2015 Underdetermined blind source separation of pipeline leak vibration signals based on empirical mode decomposition and joint approximate diagonalization of eigenmatrices. *Journal of Vibroengineering* **17** (3), 1326–1340.

Taghvaei, M., Beck, S. B. M. & Staszewski, W. J. 2006 Leak detection in pipelines using cepstrum analysis. *Measurement Science and Technology* **17** (2), 367–372.

Ting, L. L., Tey, J. Y., Tan, A. C., King, Y. J. & Abd Rahman, F. 2021 Water leak location based on improved dual-tree complex wavelet transform with soft thresholding de-noising. *Applied Acoustics* **174**, 107751. https://doi.org/10.1016/j.apacoust.2020.107751.

Wang, X. J., Lambert, M. F. & Simpson, A. R. 2005 Behavior of short lateral dead ends on pipeline transients: a lumped parameter model and an analytical solution. *Journal of Fluids Engineering, Transactions of the ASME* **127** (3), 529–535.

Xiao, R., Joseph, P. & Li, J. 2020 The leak noise spectrum in gas pipeline systems: theoretical and experimental investigation. *Journal of Sound and Vibration* **488**, 115646. https://doi.org/10.1016/j.jsv.2020.115646.

Yu, L. & Li, S. Z. 2017 Acoustic emission (AE) based small leak detection of galvanized steel pipe due to loosening of screw thread connection. *Applied Acoustics* **120**, 85–89.

Zhang, T., Zhang, Y. O. & Ouyang, H. 2015 Structural vibration and fluid-borne noise induced by turbulent flow through a 90° piping elbow with/without a guide vane. *International Journal of Pressure Vessels and Piping* **125**, 66–77. http://dx.doi.org/10.1016/j.ijpvp.2014.09.004.

Zhang, N., Xie, H., Wang, X. & Wu, B. S. 2016 Computation of vortical flow and flow induced noise by large eddy simulation with FW-H acoustic analogy and Powell vortex sound theory. *Journal of Hydrodynamics* **28** (2), 255–266. http://dx.doi.org/10.1016/S1001-6058(16)60627-3.

Zhiyan Consulting 2019 *In-depth Investigation and Investment Prospect Analysis Report of China's Urban Water Supply Industry for 2020–2026*. Beijing.

First received 31 July 2021; accepted in revised form 13 December 2021. Available online 24 December 2021